



Molecular Devices Hot Paper

International Edition: DOI: 10.1002/anie.201811515

German Edition: DOI: 10.1002/ange.201811515

Coiled-Coil Peptide Beacon: A Tunable Conformational Switch for Protein Detection

Carolyn Mueller and Tom N. Grossmann*

Abstract: The understanding of protein folding and assembly is of central importance for the design of proteins and enzymes with novel or improved functions. Minimalistic model systems, such as coiled-coils, provide an excellent platform to improve this understanding and to construct novel molecular devices. Along those lines, we designed a conformational switch that is composed of two coiled-coil forming peptides and a central binding epitope. In the absence of a binding partner, this switch adopts a hairpin-like conformation that opens upon receptor binding. Variation of the coiled-coil length modulates the strength of the intramolecular constraint. The two conformational states of this switch have been linked with characteristic fluorescent properties, which enables the detection of the receptor in real-time.

The folding propensity of proteins and their assembly into higher order structures has inspired the design of minimal peptide folds and interaction motifs.^[1] A prime example is the coiled-coil structural motif, which has emerged as a powerful tool to assemble macromolecular architectures.^[2] Coiled-coils consist of at least two α -helical peptides forming a super helix. Each peptide harbours a heptad pattern denoted as $(abcdefg)_n$ with a characteristic arrangement of polar (p) and hydrophobic (h) residues. A common pattern is $(hpphppp)_n$ in which both helices associate via a hydrophobic interface. Each of the interface residues has a specific position in a knob-into-hole manner, allowing the design of diverse coiled-coil assemblies.^[2] In heterodimeric coiled-coils the use of two different peptides, each with a characteristic arrangement of basic and acidic residues, facilitates specific and predictable interactions.^[3] For example, parallel heterodimeric coiled-coils can be assembled by placing lysine at positions “e” and “g” of one helix (basic) while equipping the same positions in the other (acidic) with glutamic acid.^[3f] The variation of the remaining residues can also be used to modulate the alignment and stability of the coiled-coils. Taking advantage of the reversible assembly of dimeric

coiled-coils, dynamic systems have been devised that give control over intermolecular coiled-coil formation.^[4] Furthermore, the grafting of helical peptide epitopes onto coiled-coils was used to enhance receptor recognition by enforcing helicity of the epitope.^[5] Intramolecular coiled-coil arrangements provide access to hairpin-like structures.^[6] In one such example, a hairpin has been designed that switches between two distinct conformations, one involving an inter- and the other an intramolecular coiled-coil.^[6a]

Often, molecular switches can adopt two defined conformations, which interchange due to an external stimulus (e.g. light or binding partner). These two different states can be linked to distinct physico-chemical properties (e.g. fluorescence intensity or catalytic activities).^[7] The hairpin architecture is one of the smallest geometries used to construct macromolecular switches. A particularly successful example involves so-called molecular beacons, which can detect the presence of certain DNA or RNA sequences.^[8] Molecular beacons are composed of DNA or DNA analogues and spontaneously adopt a hairpin-like structure. In this hairpin a central recognition motif (loop) is flanked by two complementary sequences forming an intramolecular stem. The termini of the hairpins are labeled with a fluorophore/quencher pair, resulting in low fluorescence in the closed hairpin conformation (off-state).^[8] Binding of the loop to the target nucleic acid results in hairpin opening, which triggers the separation of fluorophore and quencher, thereby resulting in increased fluorescence intensity (on-state). To broaden the applicability of molecular beacons towards protein detection, the loop was equipped with protein-binding DNA sequences^[8b,9] or peptides.^[10] As an important feature, the constraint enforced by the nucleic acid stem can be tuned via the lengths of involved sequences and thereby adjusted to the affinity of the loop/target complex.

Giving the selective binding and adjustable stability of coiled-coils, we envisioned a hairpin structure (Figure 1) fully composed of peptide modules, involving two coiled-coil helices, flanking a central peptide ligand, thereby constraining the ligand in a loop structure. In this setup, the strength of the constraint can be adjusted by varying the length of at least one of the coiled-coil helices. To allow a readout of its conformational state, the termini of the coiled-coil hairpin are equipped with a fluorophore/quencher pair (Figure 1). To ensure hairpin opening upon target binding, it is crucial to use a peptide ligand (L) which binds its receptor (R) in a conformation that is not compatible with coiled-coil formation. We based our L/R pair on the complex between MLL (mixed-lineage leukemia, aa 2840–2858)^[11] and CBP (CREB-binding protein, aa 590–670)^[12] which is involved in the transcriptional activation of numerous eukaryotic

[*] C. Mueller, Prof. Dr. T. N. Grossmann
VU University Amsterdam
Department of Chemistry & Pharmaceutical Sciences
De Boelelaan 1108, 1081 HZ, Amsterdam (The Netherlands)
E-mail: t.n.grossmann@vu.nl

Supporting information and the ORCID identification number(s) for the author(s) of this article can be found under:
<https://doi.org/10.1002/anie.201811515>.

© 2018 The Authors. Published by Wiley-VCH Verlag GmbH & Co. KGaA. This is an open access article under the terms of the Creative Commons Attribution Non-Commercial License, which permits use, distribution and reproduction in any medium, provided the original work is properly cited, and is not used for commercial purposes.

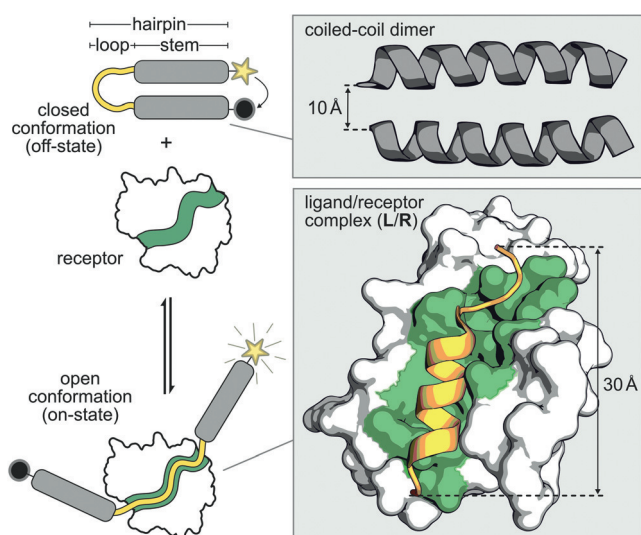


Figure 1. Coiled-coil peptide beacon in the open and closed conformation. Representation of a coiled-coil dimer (gray, PDB ID: 1kdd, including distance between analogue heptad positions *g*), and of the ligand/receptor complex (L/R, PDB ID 2lxs, distance between N- and C-terminus of ligand L (orange)).^[11] The surface area of receptor R involved in L binding is highlighted in green. The sequence of ligand L can be found in Figure 2 a).

genes.^[11] Based on an available NMR structure,^[11] we chose the 17-mer interaction motif of MLL (L, 2842–2858) as loop of the hairpin. L binds its receptor CBP (R) in a partially α -helical and extended conformation (Figure 1), resulting in a distance between the N- and C-termini of about 30 Å. This is considerably longer than the distance between the N-terminal amino acids in two interacting heptads (*gabcdef*, ca. 10 Å,^[3b]

Figure 1; Supporting Information, Figure S1). Consequently, the formation of the L/R complex would prevent coiled-coil formation. Importantly, in its unbound state, L is highly flexible,^[13] which should allow coiled-coil formation. Initially, the stability of the L/R complex was determined. For that purpose, fluorescently labeled L was synthesized on a solid-support using Fmoc-based protocols, while R was obtained by heterologous expression from *Escherichia coli* (Supporting Information, Figure S2). A fluorescence anisotropy assay revealed a dissociation constant ($K_d = 0.39 \pm 0.07 \mu\text{M}$; Supporting Information, Figure S3) in the expected range.^[14]

The hairpin stem region is based on three heptad repeats (21 amino acids per helix) of a parallel heterodimeric coiled-coil, as this is considered to be the minimal intermolecular dimerization motif.^[3f,h] Based on a parallel heterodimer reported by Woolfson and co-workers,^[3f] we designed three coiled-coil structures, all involving the same 21-mer acidic sequence (q21) but different basic peptides (Figure 2 a): A 21-mer peptide (f21) and two C-terminally truncated versions including a 17-mer (f17) and a 13-mer (f13). As fluorophore/quencher pair, fluorescein isothiocyanate (FITC) and Dabcyl were chosen. Dabcyl was attached to the acidic peptide (q21) via the ϵ -amino group of an additional C-terminal lysine. Analogously, FITC was attached to the three basic peptides (f13, f17, f21; Figure 2 a). All four labeled peptides were obtained via Fmoc-based solid-phase peptide synthesis, and the stability of the three corresponding intermolecular coiled-coils (fxx/q21) determined using a fluorescence readout. Coiled-coil formation (heterodimerization) brings fluorophore and quencher in spatial proximity, which results in reduced fluorescence intensities. Concentration-dependent fluorescence intensity measurements allowed the determination of K_d values (Figure 2 b). The two 21-mer peptides

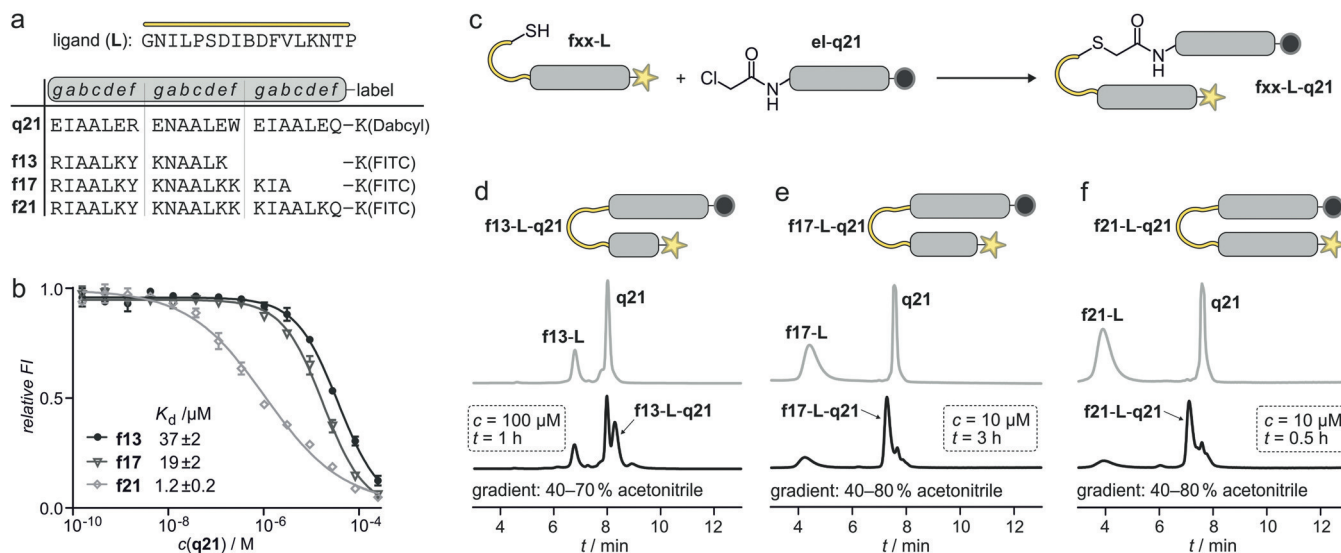


Figure 2. a) Sequences of L, q21, f13, f17, and f21 including their C-terminal labels (B: norleucine; FITC: fluorescein isothiocyanate; Dabcyl: 4-[(4-dimethylamino)phenyl]azo)benzoyl). b) Intermolecular coiled-coil formation between q21 and the three fxx peptides monitored via a fluorescence readout. Relative fluorescence intensity (*FI*) is plotted and resulting K_d values are given. Measurements were performed in triplicate (error: 1 σ) in buffer (25 mM HEPES, pH 7.4, 100 mM NaCl, 1 mM TCEP, 0.01% Tween-20). c) Ligation of cysteine-modified fxx-L with chloroacetamide-modified el-q21 providing the desired product fxx-L-q21; d)–f) HPLC traces ($\lambda = 440 \text{ nm}$ including applied gradient) before (gray) and after ligation reaction (black). Reactant concentration (*c*) and reaction times (*t*) are given (reaction buffer: 25 mM HEPES, pH 7.4, 100 mM NaCl, 1 mM TCEP).

provided the most stable complex with a dissociation constant in the expected range ($K_d(\mathbf{f21/q21}) = 1.2 \mu\text{M}$).^[3f] For **f17/q21** and **f13/q21** considerably lower stabilities were observed ($K_d = 19 \mu\text{M}$ and $37 \mu\text{M}$, respectively). To exclude interference between the coiled-coil peptides and the **L/R** complex, we performed a fluorescence anisotropy assay confirming very low affinities of all peptides for **R** ($K_d > 0.1 \text{ mM}$; Supporting Information, Figure S4).

Having verified the functionality of the isolated loop (peptide **L**) and stem region (coiled-coil), we approached the synthesis of the entire coiled-coil peptide beacon (Figure 2c). The basic peptides were N-terminally extended with the **L** sequence and equipped with an N-terminal cysteine (**fx-L**; sequences in the Supporting Information, Table S2). Peptide **q21** was N-terminally modified with chloroacetamide (**el-q21**) to facilitate a head-to-head linkage with the thiol-modified **fx-L** peptides, providing the three desired hairpins (**fx-L-q21**; Figure 2c). Initially, reactant concentrations that had previously been used in analogous intermolecular reactions ($c = 100 \mu\text{M}$) were applied.^[15] However under these conditions, only **el-q21** and **f13-L** showed sufficient solubility providing 47% product (**f13-L-q21**) after 1 h (based on HPLC, Figure 2d). Since the addition of organic solvents did not improve the solubility of **f17-L** and **f21-L** (data not shown), ligation reactions were performed at lower reactant concentrations ($c = 10 \mu\text{M}$). Under these conditions, we did not observe product formation for **f13-L** (data not shown), but obtained the desired ligation products for **f17-L** (61% **f17-L-q21** after 3 h; Figure 2e) and **f21-L** (60% **f21-L-q21** after 0.5 h; Figure 2f). These observations suggest a proximity induced acceleration of the ligation reaction, which increases with the stability of involved coiled-coils ($\mathbf{f13/q21} < \mathbf{f17/q21} < \mathbf{f21/q21}$). Based on these findings, larger reaction scales were performed to obtain the required amounts of the three ligation products (Supporting Information, methods and appendix).

First, we investigated the solubility of the peptide beacons (**fx-L-q21**), in the concentration range expected for subsequent assays, by determining their concentration-dependent fluorescence intensities. These measurements showed a linear dependency ($c = 6.25\text{--}200 \text{ nM}$; Supporting Information, Figure S5) indicating sufficient solubility. When comparing the fluorescence intensities between the three closed beacons (no receptor **R**, light gray; Figure 3a), we observed an increase in fluorescence intensity with decreasing coiled-coil length (relative fluorescence $\mathbf{f21/f17/f13-L-q21} = 1:1.3:2.1$). This increase in fluorescence is in line with the increasing distance between fluorophore and quencher due to the shortening of the basic coiled-coil peptide (Figure 2d–f). In the presence of **R** ($c = 25 \mu\text{M}$, dark gray; Figure 3a), we observed strong fluorescence increases for **f13-L-q21** (2.0-fold) and **f17-L-q21** (3.0-fold), indicating an opening of the hairpin structure. For **f21-L-q21**, this is not the case. To determine affinities between the coiled-coil beacons and **R**, we performed titration experiments applying constant beacon concentrations ($c = 100 \text{ nM}$) while varying the concentration of **R** ($c = 49 \text{ pM} \text{--} 700 \mu\text{M}$; Figure 3b). The two shorter beacons displayed sub-micromolar affinities for **R** ($K_d(\mathbf{f13-L-q21}) = 0.62 \mu\text{M}$ and $K_d(\mathbf{f17-L-q21}) = 1.27 \mu\text{M}$), while **f21-L-q21** did not provide a sigmoidal

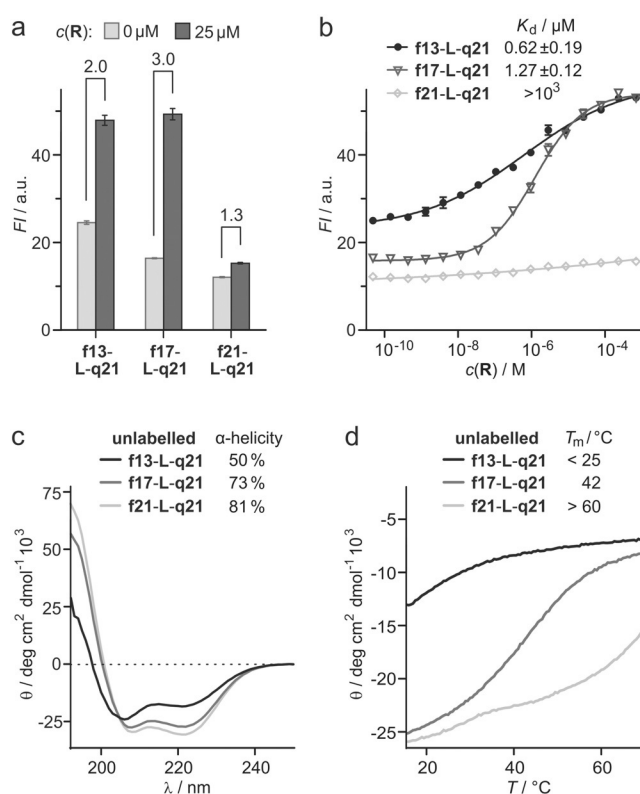


Figure 3. a) Fluorescence intensity (F) of **fx-L-q21** beacons ($c = 100 \text{ nM}$) in the absence (light gray) and presence of receptor **R** (dark gray, $c = 25 \mu\text{M}$). Factor of fluorescence increase is provided. b) Titration of receptor **R** ($c = 49 \text{ pM} \text{--} 700 \mu\text{M}$) to each **fx-L-q21** beacon ($c = 100 \text{ nM}$). K_d values are provided. All measurements were performed in triplicate (error: 1σ) in buffer (25 mM HEPES, pH 7.4, 100 mM NaCl, 1 mM TCEP, 0.01% Tween-20). c) Circular dichroism (CD) spectra (192–260 nm) of unlabeled **fx-L-q21** beacons ($c = 30 \mu\text{M}$) in 10 mM sodium phosphate buffer, pH 7.4. d) Temperature dependence of molar ellipticity (θ) at 220 nm of unlabeled **fx-L-q21** beacons ($c = 30 \mu\text{M}$, in 10 mM sodium phosphate buffer, pH 7.4).

curve, which may indicate a very low affinity for **R** ($K_d > 1 \text{ mM}$; Figure 3b). Relative to the unconstrained peptide **L** ($K_d = 0.39 \mu\text{M}$; Supporting Information, Figure S3), all hairpin structures showed a loss in binding affinity, which appeared to correlate with coiled-coil stability.

To verify intramolecular coiled-coil formation, we aimed at a characterization of the hairpin structures via circular dichroism (CD) spectroscopy. Since the labeled hairpins exhibit relatively low solubilities (ca. $1 \mu\text{M}$, data not shown), they were not suitable for CD studies. Knowing that chromophore labels tend to reduce the solubility of peptides, we considered the use of unlabeled coiled-coil hairpins. Initially, we compared the unlabeled intermolecular coiled-coils (**f13/q21**, **f17/q21**, **f21/q21**) with their labeled analogues that exhibited sufficient solubility. Notably, CD spectra and melting temperatures (T_m) were very similar for the corresponding labeled and unlabeled coiled-coils (Supporting Information, Figure S6). Consequently, the unlabeled coiled-coil hairpins were synthesized and indeed showed increased solubility. For the three unlabeled hairpins, CD spectra showed a pronounced α -helical structure (Figure 3c),

with the expected increase in α -helicity upon stem elongation (from 50 to 81 % helicity). Analogous trends were observed when comparing the T_m values of the three hairpins, revealing increasing thermal stability with increasing stem length (Figure 3d). Notably, all hairpin structures (unlabeled **fx-L-q21**) showed higher helicity and thermal stability than their intermolecular counterparts (unlabeled **f13/q21**; Supporting Information, Table S1), indicating a proximity-induced enhancement of coiled-coil stability.

To determine the hydrodynamic diameter (d) of the unlabeled coiled-coil hairpins and to investigate the presence of higher-order structures, we performed dynamic light scattering (DLS) experiments (Supporting Information, Figure S7). For **f13-L-q21** and **f17-L-q21**, these experiments revealed diameters in the expected range ($d = 3.5 \pm 0.7$ and $d = 3.7 \pm 0.7$ nm, respectively). However, for **f21-L-q21**, we observed two dominant signals: one corresponding to the monomer ($d = 3.7 \pm 0.8$ nm) and another indicating the presence of a larger species ($d = 29 \pm 9$ nm). To verify these observations, we also performed analytical size exclusion chromatography (SEC), which gave a single peak for all three hairpins (Supporting Information, Figure S8). For **f21-L-q21**, the retention volume ($V_r = 15.9$ mL) corresponded to a molecular weight of 8.8 ± 0.8 kDa, indicating the presence of a monomer (calculated $M_w = 7.0$ kDa). **f13-L-q21** and **f17-L-q21** gave slightly higher retention volumes ($V_r = 13.5$ and 15.1 mL, respectively), which is in line with their partially disordered structures.^[16] Taken together, DLS and SEC verify the monomeric character of **f13-L-q21** and **f17-L-q21**. For **f21-L-q21**, oligomerization appears to be possible (based on DLS, $c = 30 \mu\text{M}$).

Having investigated the closed hairpin conformation, we then turned to the **R**-bound open form, focusing on whether hairpin opening results in intermolecular coiled-coil formation, thereby triggering oligomerization. In particular for **f13-L-q21** and **f17-L-q21**, this is unlikely given the low intermolecular binding affinities ($K_d = 19 \mu\text{M}$ and $37 \mu\text{M}$, respectively) and the considerable fluorescence increases upon receptor binding (Figure 3b). In line with these considerations, DLS experiments showed the presence of the expected monomeric hairpin/**R** complex for both hairpins (Supporting Information, Figure S9). For **f21-L-q21**, we observe peaks with large hydrodynamic radius ($d > 20$ nm; Supporting Information, Figure S9), indicating oligomerization under these conditions. This behavior, together with low fluorescence increase upon addition of **R** (Figure 3b) and the high thermal stability, (Figure 3d) indicates a complex binding behavior for **f21-L-q21**, which was however not further investigated.

Next, we were interested to know 1) if binding of the labeled peptide beacon to **R** is reversible and 2) if the anticipated binding site on **R** is indeed targeted. For this purpose, we synthesized unlabeled peptide **L** that should compete with the labeled beacon for **R** binding. Furthermore, we chose a peptide ligand (**aL**) derived from CREB (cAMP response element-binding protein, aa 120–146),^[11] which binds **R** at an alternative binding site. A previously reported NMR structure (Figure 4a)^[11] shows the trimeric complex composed of **R**, **L** (orange) and **aL** (gray). The stability of the **aL/R** complex was confirmed using a fluorescence anisotropy

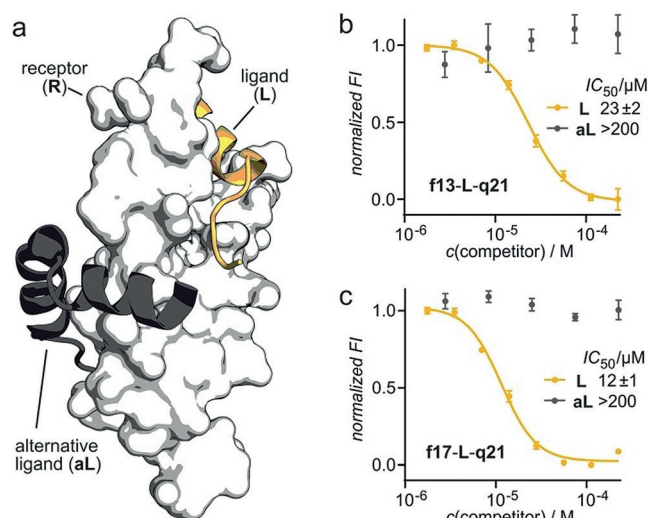


Figure 4. a) NMR structure (PDB ID: 2lxt) of the trimeric complex between **R** (white), **L** (orange), and **aL** (gray).^[11] b,c) Competition assay with preformed complex between **fx-L-q21** ($c = 100$ nM) and **R** ($c = 5 \mu\text{M}$). Normalized fluorescence is plotted and resulting IC_{50} values are provided. Measurements were performed in triplicate (error: 1 σ) in the same buffer (25 mM HEPES, pH 7.4, 100 mM NaCl, 1 mM TCEP, 0.01 % Tween-20).

assay ($K_d = 0.15 \pm 0.02 \mu\text{M}$; Supporting Information, Figure S10). For subsequent competition experiments, we chose the two coiled-coil beacons (**f13-L-q21** and **f17-L-q21**), which unambiguously bind to **R**. After complex formation, varying concentrations of **L** (orange) or **aL** (gray) were added and fluorescence intensities determined (Figure 3b and c). These measurements clearly show that peptide **L** competes with both beacons (orange, Figure 3b and c), confirming the reversibility of beacon binding. In agreement with the more stable complex between **f13-L-q21** and **R**, higher concentrations are required to compete with **f13-L-q21** ($IC_{50} = 23 \mu\text{M}$) than with **f17-L-q21** binding ($IC_{50} = 12 \mu\text{M}$). Importantly, the alternative ligand **aL** does not compete with beacon binding (gray, Figure 3b and c), confirming the site-specific binding of **f13-L-q21** and **f17-L-q21**.

Taken together, we have designed a peptide-based conformational switch composed of two coiled-coil forming peptide sequences and a central binding motif. In the absence of a binding partner, this molecular switch adopts a hairpin-like conformation that opens upon receptor engagement. The attachment of a fluorophore/quencher pair to the hairpin termini allows the detection of conformational changes in real time. We show that the length of the coiled-coil modulates the strength of the intramolecular constraint, thereby defining overall receptor affinity. This novel peptide-based switch is a minimalistic model for two competing protein–protein interactions (intra- vs. intermolecular), each linked with a distinct conformational state. Over the last years, peptide-based molecular switches, in particular photochromic ones, have been applied to study and modulate biological signaling processes and regulatory mechanisms.^[17] Along those lines, coiled-coil-based hairpins hold the potential to contribute novel chemical biology tools that are sensitive to alternative stimuli.

Acknowledgements

We are grateful to the group of Prof. H. Waldmann (MPI Dortmund) for access to the CD spectrometer and to the group of Prof. C. Czeslik (TU Dortmund) for their support and the access to DLS instrumentation. We thank the European Research Council (ERC; ERC starting grant, no. 678623) and we are grateful for support by AstraZeneca, Bayer CropScience, Bayer HealthCare, Boehringer Ingelheim, Merck KGaA, and the Max Planck Society.

Conflict of interest

The authors declare no conflict of interest.

Keywords: conformational constraint · heterodimeric coiled-coil · molecular beacons · molecular devices · protein–protein interactions

How to cite: *Angew. Chem. Int. Ed.* **2018**, *57*, 17079–17083
Angew. Chem. **2018**, *130*, 17325–17329

- [1] a) E. G. Baker, G. J. Bartlett, K. L. Porter Goff, D. N. Woolfson, *Acc. Chem. Res.* **2017**, *50*, 2085–2092; b) D. N. Woolfson, G. J. Bartlett, A. J. Burton, J. W. Heal, A. Niitsu, A. R. Thomson, C. W. Wood, *Curr. Opin. Struct. Biol.* **2015**, *33*, 16–26; c) P. S. Huang, S. E. Boyken, D. Baker, *Nature* **2016**, *537*, 320–327.
- [2] a) D. N. Woolfson, *Adv. Protein Chem.* **2005**, *70*, 79–112; b) L. Truebestein, T. A. Leonard, *BioEssays* **2016**, *38*, 903–916; c) A. N. Lupas, J. Bassler, *Trends Biochem. Sci.* **2017**, *42*, 130–140; d) F. Lapenta, J. Aupic, Z. Strmsek, R. Jerala, *Chem. Soc. Rev.* **2018**, *47*, 3530–3542; e) H. Chao, D. L. Bautista, J. Litowski, R. T. Irvin, R. S. Hodges, *J. Chromatogr. B* **1998**, *715*, 307–329.
- [3] a) T. J. Graddis, D. G. Myszkla, I. M. Chaiken, *Biochemistry* **1993**, *32*, 12664–12671; b) A. E. Keating, V. N. Malashkevich, B. Tidor, P. S. Kim, *Proc. Natl. Acad. Sci. USA* **2001**, *98*, 14825–14830; c) D. L. McClain, H. L. Woods, M. G. Oakley, *J. Am. Chem. Soc.* **2001**, *123*, 3151–3152; d) S. J. Ryan, A. J. Kennan, *J. Am. Chem. Soc.* **2007**, *129*, 10255–10260; e) G. Grigoryan, A. W. Reinke, A. E. Keating, *Nature* **2009**, *458*, 859–864; f) F. Thomas, A. L. Boyle, A. J. Burton, D. N. Woolfson, *J. Am. Chem. Soc.* **2013**, *135*, 5161–5166; g) S. Huhmann, E. K. Nyakatura, H. Erdbrink, U. I. M. Gerling, C. Czekelius, B. Kokschi, *J. Fluorine Chem.* **2015**, *175*, 32–35; h) J. R. Litowski, R. S. Hodges, *J. Biol. Chem.* **2002**, *277*, 37272–37279.
- [4] a) B. Apostolovic, H. A. Klok, *Biomacromolecules* **2008**, *9*, 3173–3180; b) F. Zhang, K. A. Timm, K. M. Arndt, G. A. Woolley, *Angew. Chem. Int. Ed.* **2010**, *49*, 3943–3946; *Angew. Chem.* **2010**, *122*, 4035–4038; c) A. M. Ali, M. W. Forbes, G. A. Woolley, *ChemBioChem* **2015**, *16*, 1757–1763; d) K. Gröger, G. Gavins, O. Seitz, *Angew. Chem. Int. Ed.* **2017**, *56*, 14217–14221; *Angew. Chem.* **2017**, *129*, 14405–14409; e) M. C. Groth, W. M. Rink, N. F. Meyer, F. Thomas, *Chem. Sci.* **2018**, *9*, 4308–4316.
- [5] a) J. M. Fletcher, K. A. Horner, G. J. Bartlett, G. G. Rhys, A. J. Wilson, D. N. Woolfson, *Chem. Sci.* **2018**, *9*, 7656–7665; b) J. H. Lee, E. Kang, J. Lee, J. Kim, K. H. Lee, J. Han, H. Y. Kang, S. Ahn, Y. Oh, D. Shin, K. Hur, S. Y. Chae, P. H. Song, Y. I. Kim, J. C. Park, J. I. Lee, *Nat. Commun.* **2014**, *5*, 3814.
- [6] a) M. J. Pandya, E. Cerasoli, A. Joseph, R. G. Stoneman, E. Waite, D. N. Woolfson, *J. Am. Chem. Soc.* **2004**, *126*, 17016–17024; b) J. D. Steinkruger, D. N. Woolfson, S. H. Gellman, *J. Am. Chem. Soc.* **2010**, *132*, 7586–7588; c) S. C. Kwok, C. T. Mant, R. S. Hodges, *Protein Sci.* **2002**, *11*, 1519–1531; d) B. F. Fisher, S. H. Hong, S. H. Gellman, *J. Am. Chem. Soc.* **2018**, *140*, 9396–9399; e) E. B. Hadley, S. H. Gellman, *J. Am. Chem. Soc.* **2006**, *128*, 16444–16445.
- [7] a) G. A. Soukup, R. R. Breaker, *Trends Biotechnol.* **1999**, *17*, 469–476; b) V. Blanco, D. A. Leigh, V. Marcos, *Chem. Soc. Rev.* **2015**, *44*, 5341–5370; c) B. L. Feringa, *Angew. Chem. Int. Ed.* **2017**, *56*, 11060–11078; *Angew. Chem.* **2017**, *129*, 11206–11226.
- [8] a) S. Tyagi, F. R. Kramer, *Nat. Biotechnol.* **1996**, *14*, 303–308; b) W. Tan, K. Wang, T. J. Drake, *Curr. Opin. Chem. Biol.* **2004**, *8*, 547–553.
- [9] a) J. J. Li, X. Fang, S. M. Schuster, W. Tan, *Angew. Chem. Int. Ed.* **2000**, *39*, 1049–1052; *Angew. Chem.* **2000**, *112*, 1091–1094; b) K. Wang, Z. Tang, C. J. Yang, Y. Kim, X. Fang, W. Li, Y. Wu, C. D. Medley, Z. Cao, J. Li, P. Colon, H. Lin, W. Tan, *Angew. Chem. Int. Ed.* **2009**, *48*, 856–870; *Angew. Chem.* **2009**, *121*, 870–885.
- [10] a) K. J. Oh, K. J. Cash, A. A. Lubin, K. W. Plaxco, *Chem. Commun.* **2007**, 4869–4871; b) S. Thurley, L. Roglin, O. Seitz, *J. Am. Chem. Soc.* **2007**, *129*, 12693–12695; c) T. Machida, S. Dutt, N. Winssinger, *Angew. Chem. Int. Ed.* **2016**, *55*, 8595–8598; *Angew. Chem.* **2016**, *128*, 8737–8740; d) E. K. Lim, K. Guk, H. Kim, B. H. Chung, J. Jung, *Chem. Commun.* **2016**, *52*, 175–178.
- [11] S. Brüsweiler, R. Konrat, M. Tollinger, *ACS Chem. Biol.* **2013**, *8*, 1600–1610.
- [12] I. Radhakrishnan, G. C. Perez-Alvarado, D. Parker, H. J. Dyson, M. R. Montminy, P. E. Wright, *Cell* **1997**, *91*, 741–752.
- [13] Y. Huang, M. Gao, F. Yang, L. Zhang, Z. Su, *Proteins Struct. Funct. Bioinf.* **2017**, *85*, 2088–2095.
- [14] a) N. Brauckhoff, G. Hahne, J. T. Yeh, T. N. Grossmann, *Angew. Chem. Int. Ed.* **2014**, *53*, 4337–4340; *Angew. Chem.* **2014**, *126*, 4425–4429; b) C. Stiller, D. M. Kruger, N. Brauckhoff, M. Schmidt, P. Janning, H. Salamon, T. N. Grossmann, *ACS Chem. Biol.* **2017**, *12*, 504–509.
- [15] M. Pelay-Gimeno, T. Bange, S. Hennig, T. N. Grossmann, *Angew. Chem. Int. Ed.* **2018**, *57*, 11164–11170; *Angew. Chem.* **2018**, *130*, 11334–11340.
- [16] V. Receveur-Bréchet, J. M. Bourhis, V. N. Uversky, B. Canard, S. Longhi, *Proteins Struct. Funct. Bioinf.* **2006**, *62*, 24–45.
- [17] R. J. Mart, R. K. Allemann, *Chem. Commun.* **2016**, *52*, 12262–12277.

Manuscript received: October 7, 2018

Accepted manuscript online: November 9, 2018

Version of record online: November 28, 2018